Energy 263 (2023) 125901

Contents lists available at ScienceDirect

Energy

journal homepage: www.elsevier.com/locate/energy

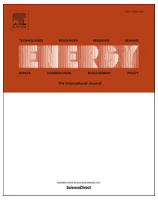

Adaptation of residential solar systems for domestic hot water (DHW) to hybrid organic Rankine Cycle (ORC) distributed generation

D.A. Rodriguez-Pastor *, J.A. Becerra, R. Chacartegui

Energy Engineering Department, Camino de los Descubrimientos s/n, Sevilla, 41092, Spain

ARTICLE INFO

Keywords:
ORC
Solar
Residential
DHW
Organic rankine
Energy storage

ABSTRACT

Among the portfolio of energy systems for local power generation, Organic Rankine cycles (ORCs) for residential applications are an opportunity for local cogeneration based on synergies with existing thermal heating and storage systems. They can be highly competitive for isolated installations and the refurbishment of existing solar heating installations based on solar domestic hot water. This article evaluates the potential for hybrid solar ORC integration in residential buildings. The analyses focus on the annual yields of a domestic 1 kW ORC cycle to assess the advantages and disadvantages of the variation of demand and the availability of solar resources. The models are developed, integrating TRNSYS and EES to allow a detailed evolution characterisation. Performance and impact of CHP adaptation are considered based on demand, storage volume-collectors area ratio, and production strategies. The analysis is completed with a thermo-economic analysis under different ranges of thermodynamic parameters. Positive IRR results of 8.61% are obtained for the installation located in Seville, Spain, operating the ORC 15% of the year. It also reduces the overheating associated with the lack of heat demand and excess solar irradiation in the solar system for the warm months by 20%.

1. Introduction/background

Heat demand for residential applications is continuously increasing [1]. This demand is currently primarily covered by fossil fuels [2], although there are relevant initiatives for decarbonisation [3,4]. Among the different alternatives are the widely used solar thermal heating and DHW systems [5]. In some cases, such as in Spain, its use is mandatory for new buildings. The technical building regulation [6], requires a minimum contribution of renewable energy to cover the thermal demand based on the surface.

It is addressed in most new buildings integrating solar thermal collectors with thermal storage tanks. According to ASIT [7], 133.5 MWth (190.650 m^2) were installed in Spain in 2020, adding up to 3.28 GWth in cumulative installed capacity, equivalent to more than 4.7 million m^2 installed and in operation. In the first half of 2021, it increased by 1% compared to the first half of 2020 [7]. Renewable heating solutions are expected to play an important role in achieving a decarbonised scenario by 2050. Solar thermal energy is expected to cover at least 10% of the final energy demand for heating and cooling in Europe [8]. The European solar thermal market is showing positive trends, and thermal installations with a high solar fraction have a high untapped potential that can be exploited by integrating new technologies. In those locations where thermal installations are designed to cover DHW and heating demands in cold periods, facilities are usually oversized in warm periods. There is an extra thermal capacity above heating or SDHW demands, and in these periods there is often a relevant electricity consumption for cooling. This is the case in many installations in Central Europe and the Mediterranean regions, which have favourable climates for this technology. Fig. 1 shows the trend in new solar thermal installations per-1000 inhabitants in Europe.

The integration of solar thermal technologies, such as ORCs, with other forms of exploiting this low-temperature renewable resource is of great interest. An organic Rankine Cycle (ORC) follows a Rankine cycle but uses a low-boiling organic refrigerant fluid as a working fluid. Depending on the operating conditions and the cycle configuration, the organic fluid can have advantages in the performance of the system and some specific com-ponents. Different organic fluids are commercially available, ranging from R134a, R600a, R245fa to azeotropic fluids [9]. The main advantages of the ORC with respect to the conventional Rankine cycle are reduced temperature and critical pressure, allowing thermal recovery at low temperatures with higher efficiencies at these conditions.

* Corresponding author.
E-mail address: drodriguez4@us.es (D.A. Rodriguez-Pastor).

https://doi.org/10.1016/j.energy.2022.125901
Received 31 January 2022; Received in revised form 21 October 2022; Accepted 25 October 2022
Available online 7 November 2022

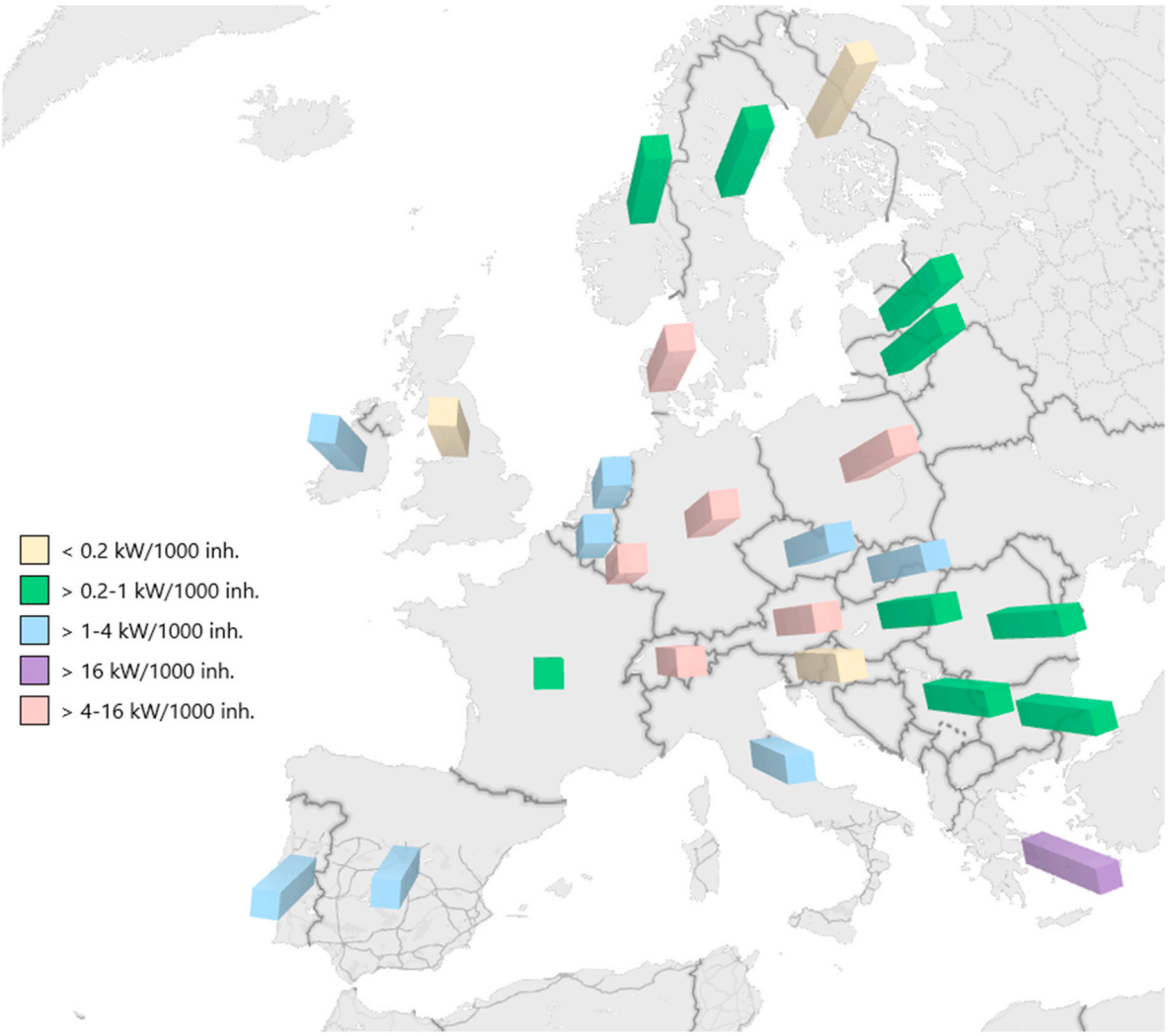

Fig. 1. New solar installed capacity in 2018 in kWth per 1,000 inhabitants – EUROPE (Source: AEE, INTEC, SHC (2020)).

An adequate integration would allow the generation of electrical energy from the thermal energy of, for example, degraded effluents in an industry or DHW in buildings using low-boiling-temperature organic fluids [10]. This integration of the ORCs in microdistributed generation (micro-DPG) occurs in the power range from watts to 5 kW. In the context of solar ORCs, M.A. Ancona et al. [11] studied the alternative use of other refrigerants with low GWP, identifying R513A as the best alternative to R134a. J.S. Pereira et al. [12] concluded the interest in micro-ORCs in the residential sector due to their capability to adapt to fast changes in demand loads, and the evaporator design plays an important role. The works of Pei et al. [13] and Antonelli et al. [14] used parabolic trough collectors, presenting ORC thermal efficiencies of 8.6% with regeneration and 4.9% without regeneration [13] using collectors of low concentration ratio and R123 as working fluid. They identified a significant dependence of the thermal performance of the ORC on the saturation of the refrigerant. Fresnel solar reflectors have also been studied at the residential level for ORC power production, as in the case of Arteconi et al. [15] by trigeneration, where power outputs of 26% higher than in the base case (2 kWe ORC CHP) were obtained, and savings of 9% were predicted using phase change storage. ORCs can also be implemented in cogeneration plants with absorption chillers [16], with average annual overall cogeneration efficiencies of 32%–42% [17]. Martinez et al. [18], used TRNSYS to model cogeneration systems coupled to MATLAB with two-axis solar tracking systems. Villarini et al. [19] highlighted the potential of ORC-based trigeneration under different radiation conditions in two Italian locations. In Lizana et al. [20], the potential benefits of latent heat integration were obtained to improve micro-ORC performance, predicting a cost reduction of 50% compared to a pressurised water tank for energy storage.

This article aims to evaluate the impact of using ORC systems for electricity production in buildings with solar water heating systems, taking advantage of existing elements. Thus, the possible penalty for demand and the thermal and economic benefit obtained after the implementation of micro-ORC in existing solar domestic hot water systems is evaluated. This is done by analysing the solar fraction for both the base case without the organic Rankine cycle and the system proposed in this work. TRNSYS is used for the dynamic simulation of the system and is linked to an EES model for the thermodynamic calculation of the ORC. Optimal operating points that maximise electricity generation without compromising water demand are discussed. Several operating strategies are proposed as a function of consumption in a house in the south of Spain. Detailed analyses of the effect of the water storage volume, the size of the solar installation, and the installation costs are carried out.

2. Methods

This work analyses the integration of ORC in residential applications using thermal energy storage in hot water that is also used for DHW and heating. An example of the integration layout is presented in Fig. 2. This

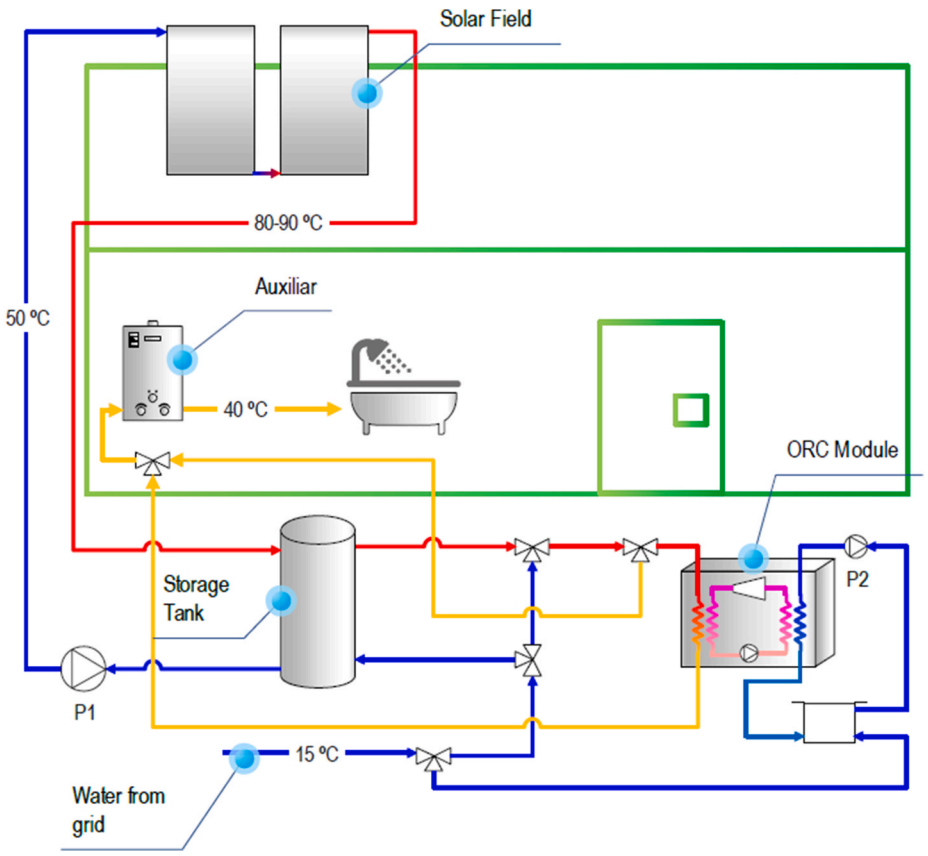

Fig. 2. ORC-SDHW system adaptation layout.

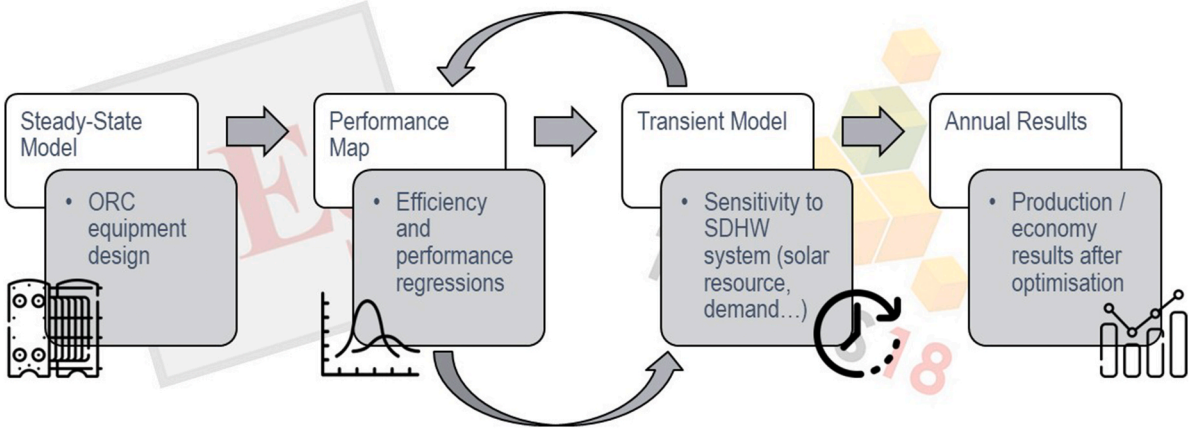

Fig. 3. Block diagram of the proposed methodology for the simulation of the ORC- SDHW integration.

is a typical SDHW diagram of a residential application, including an additional intermediate evaporator to harness the energy. To not penalise the demand and to ensure that the production of energy in the expander does not have an adverse effect on the consumer, three-way valves and thermo-valves are considered, which will be controlled according to the irradiation conditions and the outlet temperature of the collectors and the storage water tank. Under an excess of available energy over the demand, determined by a setpoint temperature placed in the solar loop, the ORC pump will be activated to produce electrical energy and lower the temperature of the water circuit, stabilising the demand.

For simulating the performance of the system, the methodology seeks a compromise between the accuracy of the calculations, the computational cost, and the convergence of the method. Several considerations regarding control and possible operating modes were considered to evaluate the preliminary behaviour of a dynamic ORC system. They are discussed in the next section. For the simulation, the models developed within different software were linked to establish cost-optimal designs for the ORC-SDHW integration under an annual base evaluation (Fig. 3).

The calculation process is shown in the flow chart in Fig. 4. In this sense, the ORC is modelled in a steady state with EES. Performance regressions are obtained as a function of the evaporation temperature, which depends on the instantaneous solar resource and the domestic hot water demand. After obtaining the results, they are compared in a Python code that groups the annual hourly costs of the electricity market,

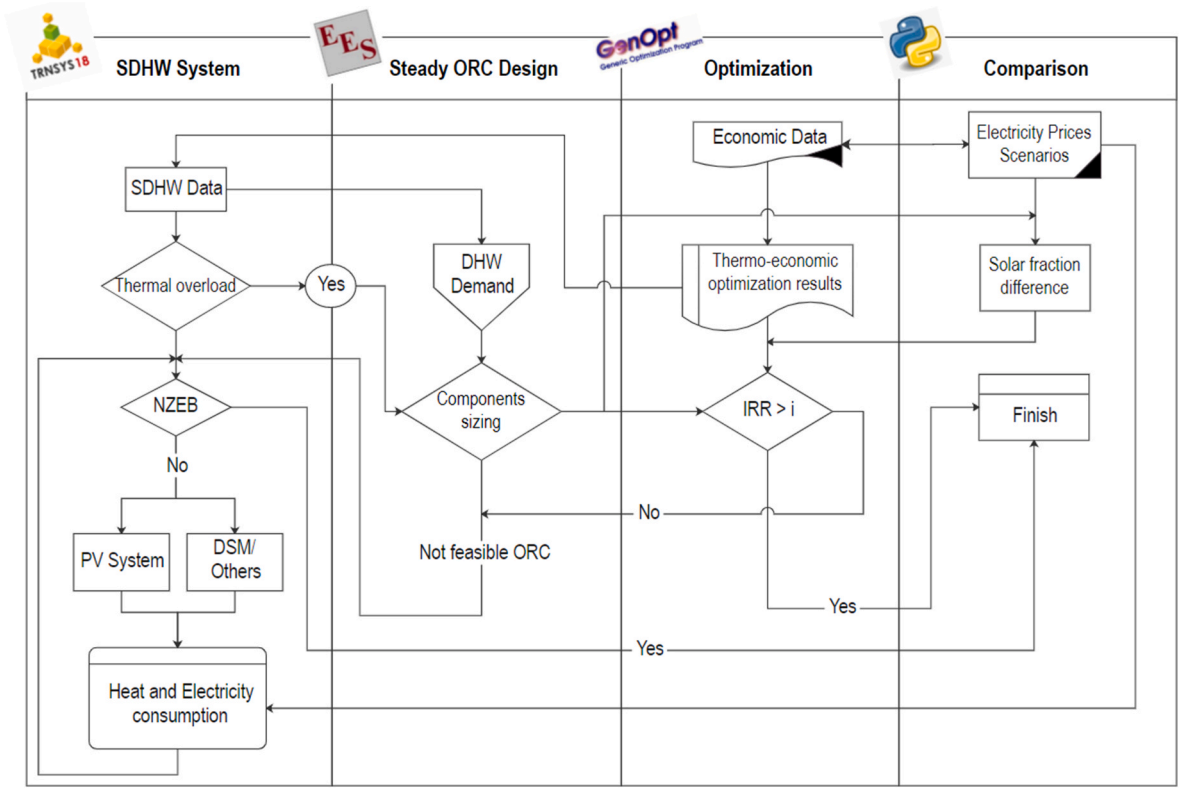

Fig. 4. Flow chart of the optimisation and decision-making process carried out.

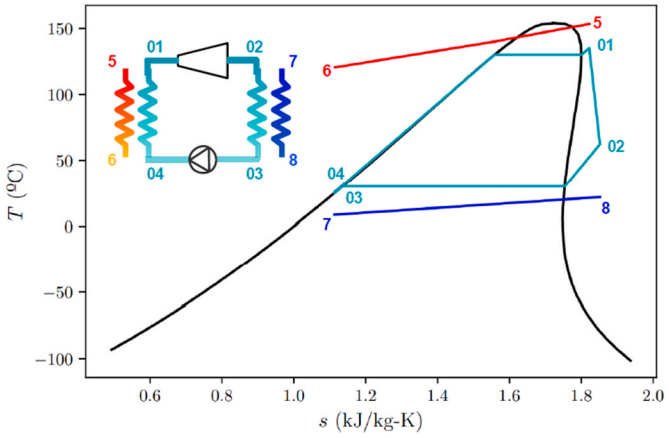

Fig. 5. T-s diagram for R245fa working fluid.

which will be used to evaluate the benefits associated with the self-consumption achieved with the integration of the micro ORC within the installation.

Flat plate collectors reach maximum temperatures on the order of 85–90 °C, which can be reduced by including a storage system. There are many overly large installations in the Mediterranean region, with heating winter designs and correcting the demand for summer. This produces an excess of thermal energy that, in most cases, can only be reduced by covering the collectors.

ORCs are usually implemented in applications with higher waste heat ratios, due to their high prices, appealing to medium or high temperatures (combustion gases, product flow, or water flow) in industries where viabilities are obtained [21]. This work proposes their integration into existing thermal solar installations, taking advantage of existing systems. It allows the use of a low-temperature thermal source, allowing curtailments in times of high solar irradiation, such as summer in the Mediterranean region, and taking advantage of the installed collectors. The energy available in excess over the demand can be exploited by the organic Rankine cycle that can lower the water temperature in the collector by 30–35 °C (depending on the mass flow rate) as it passes through an intermediate evaporator, improving demand and producing electrical energy in a renewable way.

In this work, to integrate ORC into existing installations and adapt them to optimal operation, different fluids can be selected for the cycle [22]. Based on previous work, in this application [23,24] R245fa has been selected as the working fluid. Fig. 5 shows the thermodynamic processes of the selected cycle.

The models are used to estimate the performance in different climatic zones in Europe based on monthly temperatures [25] and meteorological data [26], assessing the viability of micro-ORCs in residential applications with solar thermal facilities in these regions.

2.1. Steady-state model

The ORC steady-state model has been implemented in EES [27]. It has been used to size the equipment and the overall heat transfer coefficients of both the evaporator and the condenser.

2.1.1. Evaporator

Water from a low-temperature heat source will enter a three-zone evaporator [28]. The two-phase heat transfer is given by the correlation for the evaporation of a fluid in a plate heat exchanger based on the dimensionless Nusselt number (Nu_{tp}) given by the work of Amalfi et al. [29]:

$$Nu_{tp}(Bd<4) = 982 \cdot \beta'^{1.101} We_m^{0.315} Bo^{0.320} \rho'^{-0.224} \quad (1)$$

$$Nu_{tp}(Bd \geq 4) = 18.495 \cdot \beta'^{0.248} Re_v^{0.135} Re_{l,sat}^{0.351} Bd^{0.235} Bo^{0.198} \rho'^{-0.223} \quad (2)$$

For x = 1 or saturated vapour, it is convenient to use Martin's

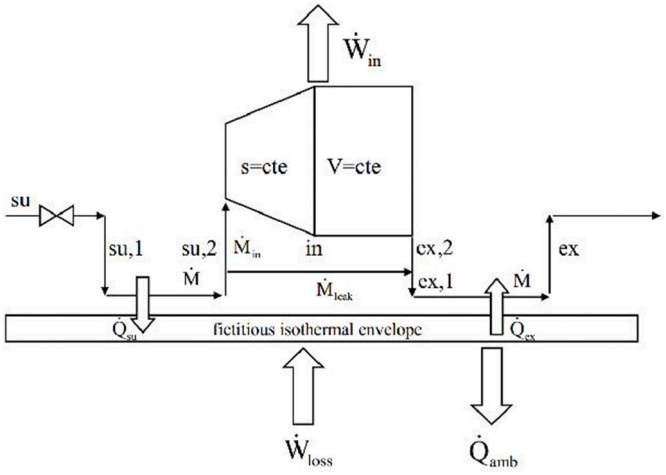

Fig. 6. Semi-empirical model of the scroll expander. Lemort et al. [31].

correlation for a single phase (Nu_v) in a plate heat exchanger [30]:

$$Nu_v = 0.122 \cdot Pr^{1/3} \left(\frac{\mu}{\mu_{wall}}\right)^{1/6} \left(f \cdot Re^2 \sin(2\beta)\right)^{0.374} \tag{3}$$

For the calculation of the pressure drop Δp_{fr} in the evaporator, the two-phase friction factor coefficient proposed by Amalfi et al. [29], as a function of the corrugation angle f and for each step Δy in the evaporator, will be used:

$$\Delta p_{fr} = \frac{2fG^2 \Delta y}{d_h \rho_m} \tag{4}$$

2.1.2. Expander

For the open-drive scroll expander, a model proposed by Lemort et al. [31] and which has been widely used and referenced in Refs. [32–34] is used. This model separates the refrigerant evolution into two main working zones, one isentropic and the other isochoric (see Fig. 6).

The thermodynamic processes that then occur are as follows.

- Inlet pressure drop (su→ su,1)
- Inlet cooling (su,1 → su,2)
- Isentropic expansion is given by the built-in volume ratio of the expander to the internal pressure. (su,2 → in)
- Isochoric expansion up to the outlet or condensing pressure. (in → ex,2)
- Mixing of suction and leakage flow. (ex,2 → ex,1)
- Cooling or heating at the outlet of the expander. (ex,1 ex) The mass flow from the inlet to the expander shall be the difference between the refrigerant flow rate from the evaporator and the mass fraction due to leakage.

The internal flow will be a function of the swept volume V_s of the expander and its rotational speed N, divided by the specific volume of the working fluid under evaporating conditions $v_{su,2}$.

$$\dot{M}_{su} = \dot{M} - \dot{M}_{leak} = \frac{N \cdot V_s}{60 \cdot r_{v,su} v_{su,2}} \tag{5}$$

The internal expansion power is given by the isentropic and isochoric processes mentioned:

$$\dot{W}_{in} = \dot{M}_{su}\left(\left(h_{su,2} - h_{su}\right) + r_{v,su} v_{su,2} \left(p_{su} - p_{ex}\right)\right) \tag{6}$$

The mechanical loss torque T_m will be a characteristic of the expander, where the losses:

$$\dot{W}_{loss} = 2\pi \cdot N \cdot T_m \tag{7}$$

Table 1
Coefficients for estimating expander efficiency as a function of evaporating temperature in Equation (14).

Evaporation Pressure	a (–)	b ($°C^{-1}$)	c ($°C^{-2}$)	d ($°C^{-3}$)
8 bar	−5.421	0.126	$-8.6 \cdot 10^{-4}$	$2.49 \cdot 10^{-6}$
9 bar	−5.871	0.135	$-9.3 \cdot 10^{-4}$	$2.62 \cdot 10^{-6}$
10 bar	−6.432	0.146	$-1.01 \cdot 10^{-3}$	$2.8 \cdot 10^{-6}$

2.1.3. Condenser

A heat sink is required to bring the working fluid to its liquid state, absorbing the excess energy at the outlet of the expander. To characterise the condenser, a three-zone model is also developed. The correlation of the transfer coefficient $h_{l,sat}$ is given by Ref. [35]:

$$h_{l,sat} = 1.875 \cdot \Phi \left(\frac{k_l}{d_h}\right) Re_{eq}^{0.445} Pr_l^{1/3} \tag{8}$$

Furthermore, the calculation of the pressure drop (Δp_{fr}) is given as a linear function of the kinetic energy K [35] obtained experimentally:

$$\Delta p_{fr} = 1.9 \frac{K}{V} \tag{9}$$

where:

$$K = V \frac{G^2}{2\rho_m} \tag{10}$$

2.1.4. Pump

The pump is modelled assuming constant volumetric efficiency and varying the isentropic efficiency as a function of the isentropic (measurable) power [34]. From these coefficients and an imposed rotational speed (N_{pump}), plus a given displacement volume V_s as a function of the manufacturer pump, the mass flow rate $\dot{m}_{in}$ is estimated:

$$\dot{m}_{in} = \rho_{in} V_s \frac{N_{pump}}{60} \varepsilon_{vol} \tag{11}$$

$$\dot{W}_{pump} = \frac{\dot{m}_{in} v_{in} (p_{out} - p_{in})}{\varepsilon_{is}} \tag{12}$$

2.2. Transient-state analysis

Transients have been modelled in TRNSYS. The unsteady model includes the pump based on equations (11) and (12), which allows it to regulate the mass flow rate appropriately according to radiation at a given moment and therefore on the temperature of the water inlet to the evaporator, obtain ideal conditions for the cycle, and obtain the maximum electrical power without penalising demand.

The detailed stationary models were adapted to simplified models with algebraic equations, considering that the equipment operates under partial load. The adaptation to these models has been carried out based on [36], to obtain the global coefficients in the evaporator and condenser. The overall transfer coefficient U for both heat exchangers shall be as follows:

$$U = U_{nom} \left(\frac{\dot{m}}{\dot{m}_{nom}}\right)^n \tag{13}$$

where n takes values of 0.5 for the evaporator and 0.4 for the condenser.

The isentropic efficiency of the expander ε_{is} is given by a third-order regression of an open drive scroll expander model in the EES software [37]:

$$\varepsilon_{is} = a + bT_{ev} + cT_{ev}^2 + dT_{ev}^3 \tag{14}$$

Where the coefficients a, b, c and d are obtained from the sensitivity analysis for 1000 points (R = 99.99%) as a function of the imposed

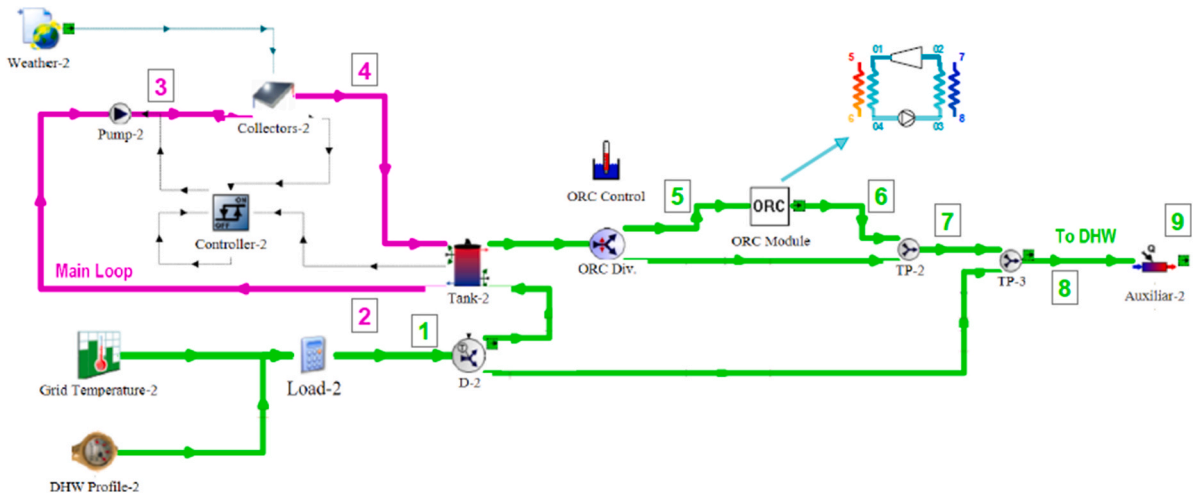

Fig. 7. TRNSYS Simplified layout with SDHW-ORC adaptation.

Table 2
Collectors specification.

Parameter	Value	Units
Collector area	5.7	m^2
Fluid specific heat	4.19	$kJ/kg-K$
Efficiency mode	1	–
Tested flow rate	0.011	$kg/s-m^2$
Intercept efficiency (a_0)	0.801	–
Efficiency slope (a_1)	3.93	W/m^2-K
Efficiency curvature (a_2)	0.026	W/m^2-K^2
1st-order IAM	0.2	–

evaporating temperature T_{ev}. The temperature dependence is selected for simplicity in the TRNSYS code. Table 1 shows the results of the analysis on the estimate of expander efficiency as a function of the evaporating temperature for different working pressures (Eqn 14).

When using the CoolProp libraries [38], the state of the working fluid is calculated from the desired set points in the differential control of the entire plant.

3. SDHW-ORC adaptation

3.1. Simulation

Fig. 7 presents the installation layout to be simulated in the TRNSYS environment, where different aquastat-based control types are implemented for the ORC and hysteresis for the solar collector circuit.

The simulations in TRNSYS will be based on Types 4 and 1 [39] for the storage tank and the collectors, respectively. The equations modelling the system are algebraically simplified in TRNSYS.

$$\eta_{coll} = a_0 - a_1\frac{\Delta T}{I_T} - a_2\frac{(\Delta T)^2}{I_T} \tag{15}$$

For the particularisation of solar collection and storage elements, the parameters that model the behaviour of the equipment at a thermodynamic level are shown in Table 2, in which three parameters give the efficiency of collectors: a_0, a_1, and a_2, according to the ASHRAE, SRCC, and CEN standards

The definition of the simulation for the base case (Fig. 8) is given by the following layout:

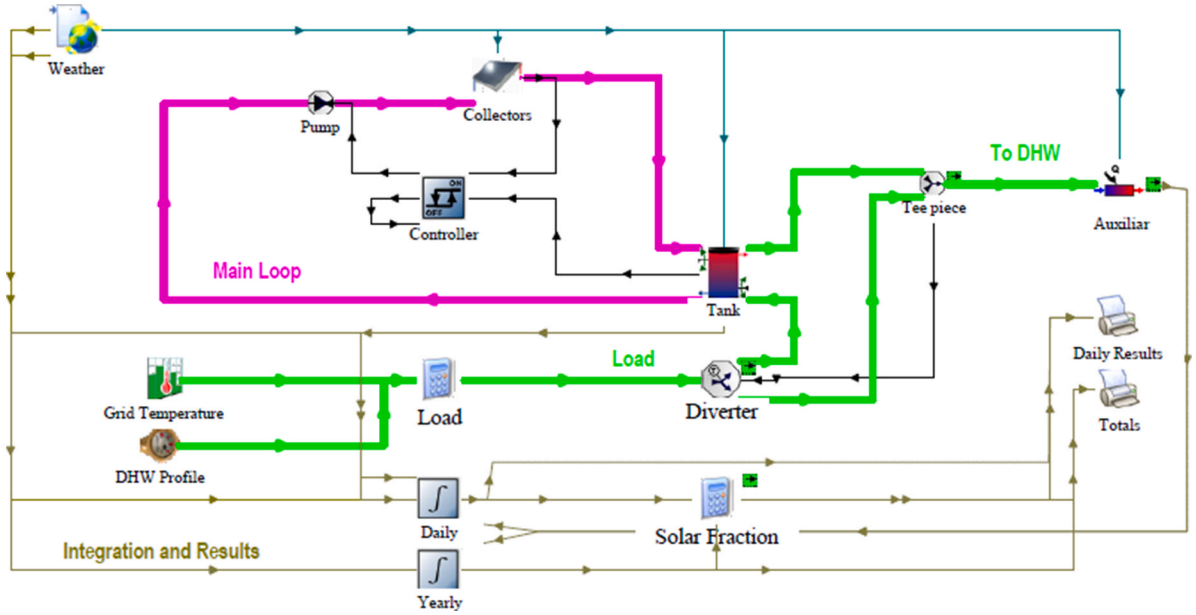

Fig. 8. SDHW TRNSYS layout.

Table 3
Mass and energy balances for all the points in the plant and the time dependence of the thermodynamic parameters.

State	Loop	$\dot{m}$ (kg/hr)	T (°C)	p (bar)	$\dot{Q}$ (kW)	$\dot{W}$ (kW)	Control Signal
1	Solar	Load at time t	From grid (11–20 °C) at time t	$f(Grid, \dot{m}_{load})$	–	–	–
2		$f(T_{out.coll})$	45	$f(Grid, \dot{m}_{load})$			Hysteresis from controller 2
3		$f(T_{out.coll})$	45	$f(Grid, \dot{m}_{load})$	–	$\dot{m}\,\Delta p/10$	Hysterisis from controller 2
4		$f(T_{out.coll})$	$f(T_{in,coll}, T_{amb}, I)$	$f(Grid, \dot{m}_{load})$	$\dot{m}_2 C_p (T_{out,coll} - T_{in,coll})$	–	–
5		$f(T_{load})$	$f(T_{in,coll}, T_{amb}, I)$	$f(Grid, \dot{m}_{load})$	$\dot{m}_1 C_p (T_{load} - T_1)$	–	Aquastat ORC
6		$\dot{m}_5$	$f(T_{04}, \dot{m}_{load})$	$f(Grid, \dot{m}_{load})$	$\dot{m}_5 C_p (T_6 - T_5)$	–	Rotation Speed from DHW controller
7		$f(T_{load}, ORC_{control})$	$f(T_{load}, T_6, \dot{m}_{ref})$	$f(Grid, \dot{m}_{load})$	–	–	Aquastat ORC
8		$\dot{m}_1$	$f(T^{set}_{DHW}, T_6, \dot{m}_{ref})$	$f(Grid, \dot{m}_{load})$	–	–	Diverter 2
9		$\dot{m}_1$	$f(T^{set}_{DHW})$	$f(Grid, \dot{m}_{load})$	$\dot{m}_1 C_p (T^{set}_{DHW} - T_8)$	–	Tee Piece 3
1	ORC	$f(N_{pump})$	$f(T_5, \dot{m}_5)$	$8 - \Delta p_{ev}$	$\dot{m}_{ref}(h_1 - h_4)$	–	Rotation Speed from DHW controller
2		$f(N_{pump})$	$f(\epsilon_{exp}, \dot{m}_{ref})$	1.2	–	$\dot{m}_{ref}(h_2 - h_1)$	Aquastat ORC
3		$f(N_{pump})$	Saturation temperature at p_3	$1.2 - \Delta p_{cd}$	$\dot{m}_{ref}(h_2 - h_3)$	–	–
4		$f(N_{pump})$	$f(\dot{W}_{pump})$	8	–	$\dot{m}_{ref}(h_4 - h_3)$	Aquastat ORC

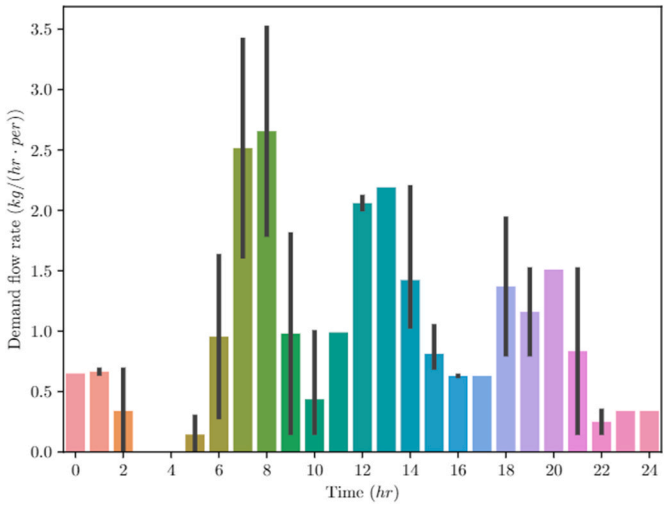

Fig. 9. Hourly DHW demand flow rate estimation by person. The black bars indicate an increase in demand for peak winter periods.

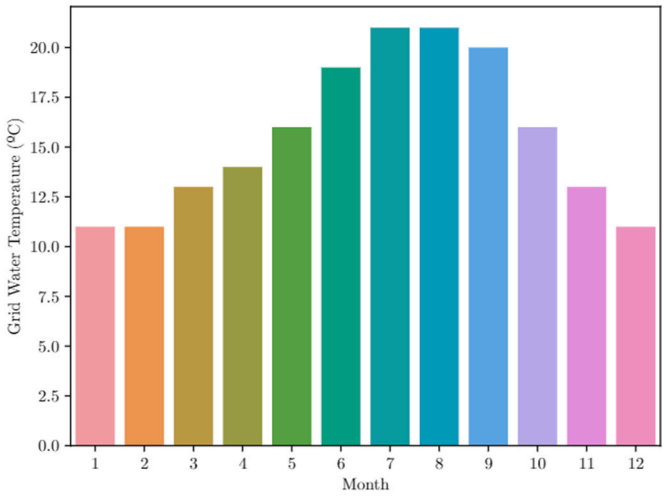

Fig. 10. Main water temperature (°C) by month in Seville.

The temperature set point at the tank outlet will determine the fraction of water at the tank outlet that will pass through the cycle, diverting the mass flow to the mixing valve if there is no excess thermal energy. Another diverter valve determines, based on a tank temperature control, the fraction of main water in the storage tank or for mixing with cold water if the domestic hot water temperature is exceeded. The mass and energy balances per point are shown in Table 3. In it, the different thermodynamic parameters are established as a function of the temperatures and characteristics of the grid water (*Grid*), as well as other variables associated with the ORC, such as efficiencies, mass flows, or rotational speeds.

This work considers that TERMICOL provides the collectors and that the model is T20US. On the other hand, the storage tank has 0.3 m^3 with six stratification levels, and the height h is calculated for each instant in time based on an estimate given by the manufacturer.

$$h = 0.32 \cdot V_{tank} + 1.3\ [m] \tag{16}$$

with a maximum tank height of 1.4 m (0.3 m^3) and a thermal loss coefficient of 0.694 W/m^2K.

$$\frac{dT_{tank}}{dt} = \frac{(\dot{Q}^{in}_{tank} - \dot{Q}^{out}_{tank})}{C_{tank}} \tag{17}$$

Through Type 15, meteorological data files will be uploaded to study the climate, with the aim of obtaining a European production map and a feasibility map for this adaptation. In this article, the location of Seville in southern Spain is detailed in more depth, with variable main water and thermoeconomic optimisation. For the rest of the regions, this main water temperature will be taken as a constant throughout the year and the condensing pressure will be set at 1.8 bar and 8 bar for the evaporating pressure. The demands are considered on an hourly basis. Occupancy will be assumed to be invariable throughout the year (Fig. 9), where two scenarios are defined according to the season (summer or winter), and demands in the cold months are assumed to be higher at certain times of the day (black bars in Fig. 9). This assumption is made for a single-family dwelling application, but it should be reformulated for other occupation profiles, such as tertiary buildings (i.e., hotels). This means a greater performance of the collector system, which does not necessarily favour the ORC, so we have a smaller performance margin for this cycle. If the demands were reduced, the water temperature would be higher, which would allow the cycle to have higher saturation temperatures, or in our case, the mass flow would be higher for a fixed pressure, thus obtaining greater power in the expander. The time step is hourly, despite the large variability in consumption, for simplicity and because the objective of this work is the annual evaluation of the ORC-SDHW integration.

The monthly temperature of the main water is given by ATECYR [25] and is represented in Fig. 10. In the summer months (July and August in particular), the mains temperature reaches 20 °C, which reduces the useful heat to be delivered by the collectors.

3.2. Minimisation of the difference in solar fractions, transient multiobjective optimisation

A multiobjective optimisation process was performed based on

Table 4
Cost of ORC components as a function of basic thermodynamic and geometrical parameters [32] [33],

Component	Costs (€)
Expander	$(300 + 170 \cdot \dot{V}_{su}) \cdot 3$
Heat Exchangers	$A \cdot 310 + 200$
ORC Pump	$900 \cdot (W_{pp}^{ele}/350)^{0.25}$
Liquid receiver	$l \cdot 15 + 31.5$
Piping	$(1 + 0.2 \cdot d_t) \cdot L_t$
Refrigerant	$18 \cdot M$
Valves	60
Control	600
Hardware	300
Assembly	$25\% \cdot \sum_{i=1} C_i$

TRNOPT. It is presented as a TESS [40] plugin for TRNSYS that allows the optimisation of the different parameters of the installation. It has been used to evaluate the benefits associated with the adaptation of the solar installation with the addition of the ORC system, and the losses due to the auxiliary differences are defined. The total life cycle cost will also be considered based on the dimensioning of the cycle. Costs will be given by the expressions provided by Quoilin et al. [33] and Garcia-Saez et al. [32] and updated to date 2021 for each component in Table 4.

To determine the economic viability of the installation, optimisation of the thermodynamic variables is necessary, as long as the benefits are also maximised. These gains are given by the net power production of the ORC and the difference in the auxiliaries that can be produced (Eq. (18)). The improvement in economic terms considers the hourly electricity market price in 2020, according to OMIE [41], with an average electricity price of 0.1215 €/kWh after taxes. To not increase the initial cost and cycle performance, optimisation constraints are established based on previous work [24], also considering the construction limits of the solar loop equipment. The condensation process is assumed to occur at ambient temperature (25 °C) and atmospheric pressure or higher to facilitate the design and operation of the installation. Similarly, the evaporation pressure has a maximum value of 10 bar to avoid raising the evaporation temperature, given the heat input (water from the collectors) at low temperature (<90 °C). It is assumed that the demand is less than 120 l/day, given the occupancy characteristics of the house taken for the case study. A factor that increases the mass flow through the ORC, given by the pump speed, is also included. Finally, the temperature of the water set point that activates the ORC control varies between 75 and 90 °C, due to the construction characteristics of flat plate solar collectors.

$$\begin{aligned} &\max_{pev,pcd,m_{load},N_{pp},T_{set}^{ORC}} \left(\left(W_{\exp} - W_p \right) - \left(Q_{aux}^{ORC} \right) \right) P_{el} \\ &s.t \quad 8 \geq p_{ev} \geq 10 \ \ bar \\ &\quad 1 \geq p_{cd} \geq 3 \ \ bar \\ &\quad 112 \geq m_{load} \geq 120 l/day \\ &\quad 1 \geq f_{N_{pp}} \geq 1.5(-) \\ &\quad 75 \geq T_{set}^{ORC} \geq 90^{\circ} C \end{aligned} \tag{18}$$

With P_{el} the hourly electricity price in €/kWh, m_{load} the daily demand in litres per day and $f_{N_{pp}}$ a pump speed increase factor, which will condition the mass flow rate of the cycle.

In this way, the TRNSYS plugin will perform a series of simulations until it finds the maximum benefit based on the Hookes-Jeeves method. Variation in ORC parameters will be important to the overall evaluation of the facility, as will be discussed later. The performance of the solar collector system will vary as the output of the microgeneration system varies. In addition, there will be a conflict between the price of electricity and the cost overrun associated with the difference in auxiliaries, so the feasibility of retrofitting should be studied from this point of view. The lower set point will ensure higher ORC production, but it will always depend on consumption and weather conditions, which does not guarantee a higher profit based on both parameters (Fig. 11). For the same condensing pressure, the most beneficial operating point is 77.5 °C, which provides some evaporation of the refrigerant from the cycle, but it will not be total. Therefore, the refrigerant will reach the volumetric expander with a significant percentage of liquid that could be detrimental to its operation in the long term. For this reason, the economic analysis considers a 2% annual cost due to the maintenance of the installation. The most significant benefits are obtained based on the lower condensation pressure and an intermediate temperature point at the storage tank outlet, which indicates some robustness of the control

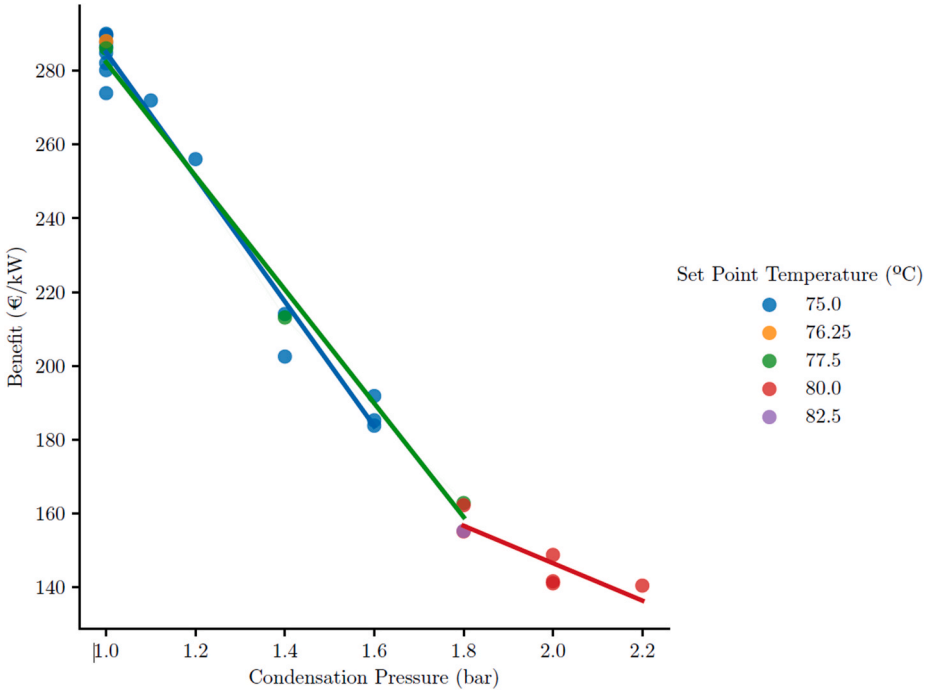

Fig. 11. Optimisation results as a function of condensing pressure and operating point of the ORC.

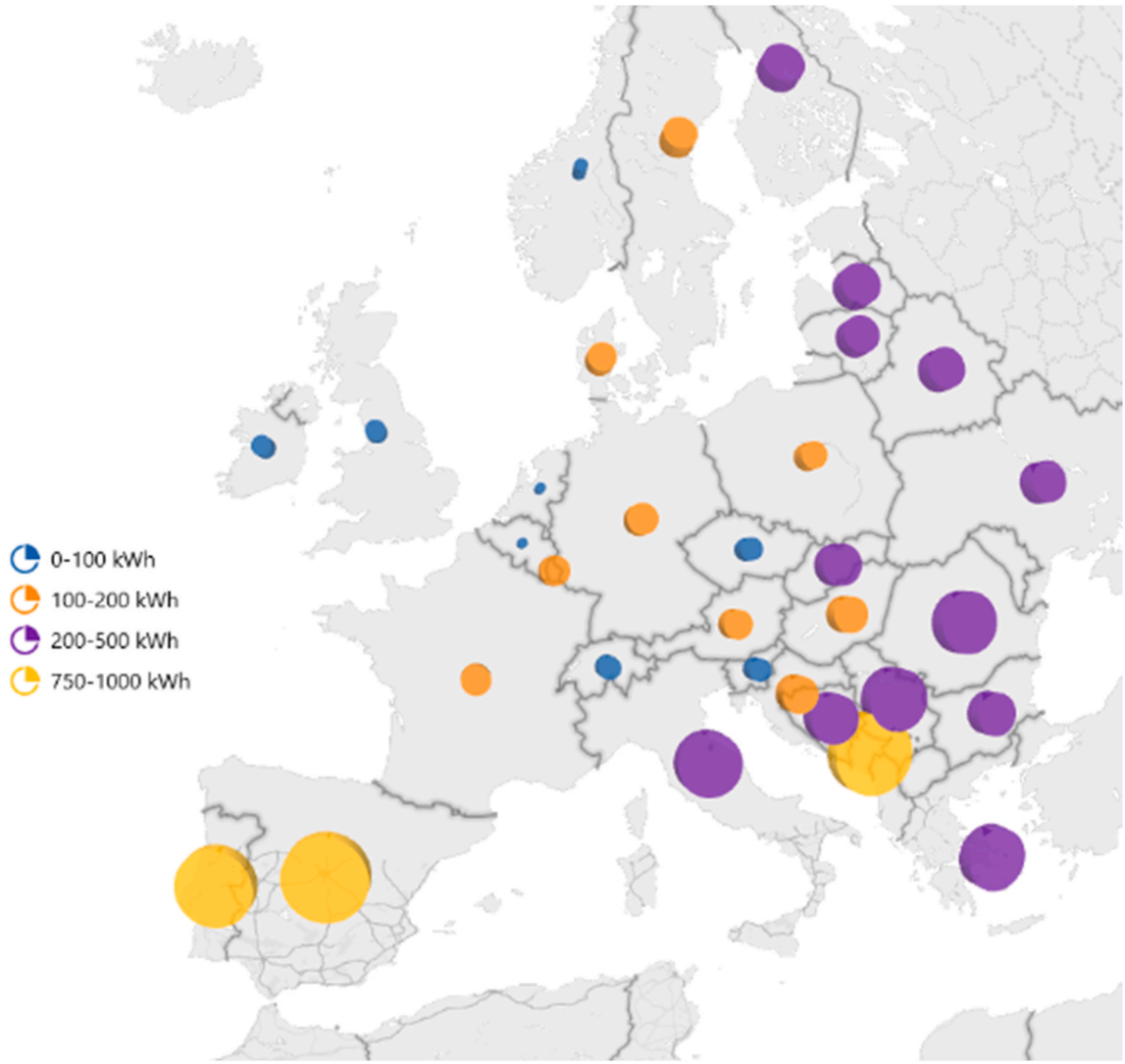

Fig. 12. SDHW-ORC Proposed Annual installation production by country in Europe.

acting on the pump, modifying the mass flow through the cycle based on the pump speed.

Given the variability in electricity costs, there are times when the electrical production of the ORC compensates for the costs due to the variation in the auxiliaries. The auxiliaries will be given based on the electricity consumption and no account of gas boilers or similar will be taken.

There is a range for 77.5 °C water temperature at the outlet for which the profit can fluctuate considerably due to price uncertainty. Condensing pressure limits production by decreasing the expansion ratio of the cycle and, with it, production, despite decreasing refrigerant pumping costs. Therefore, for higher water outlet temperatures from the storage tank, higher evaporation pressures are desirable, which increase the energy extracted by the expander and the efficiency of the Rankine cycle. However, this option is not suitable for lower temperature set points, as it reduces the efficiency of the cycle, and the water that leaves the tank does not have sufficient heat capacity to evaporate the refrigerant.

4. Results and discussion

According to the climate in Europe, the preliminary results of ORC production (Fig. 12) show that the solar potential is high enough in the Mediterranean area to have a surplus of useable thermal energy. It is worth noting the production of the continental climate, which is about five times lower than the climate mentioned above. Likewise, the alpine climate has a production that can reach 500 kW h per year without penalising the demand, given its meteorological conditions. The boreal climate also stands out, with an annual production of around 250 kW h, indicating the potential of ORCs, despite the low demand for a single-family home and the limited solar resources in these climates.

Compared with the average annual irradiation of each European capital, considering the temperature differences associated with the climate of each region, a linear regression of the estimated production is performed based on this average parameter:

$$W_{ORC} = -621.93 + 0.64 \cdot \overline{H} \pm 111.83 \quad (19)$$

Where W_{ORC} is the annual ORC production in kWh and $\overline{H}$ is the average annual irradiation in kWh/m^2. Where the regression is fitted to a point cloud simulated with TRNSYS, resulting in $R^2 = 86.4\%$. From this linear regression, the suitability of the installation according to the European climate is estimated in the simplest way. Therefore, given a greater solar resource and based on the local trend, Seville in southern Spain will be studied in more detail, with 16.936 MJ/m^2-day of monthly average global radiation and 18.8 °C of average temperature. In the summer months, a typical day performance in this region is shown in Fig. 13. The production trend decreases as the load on the water storage tank

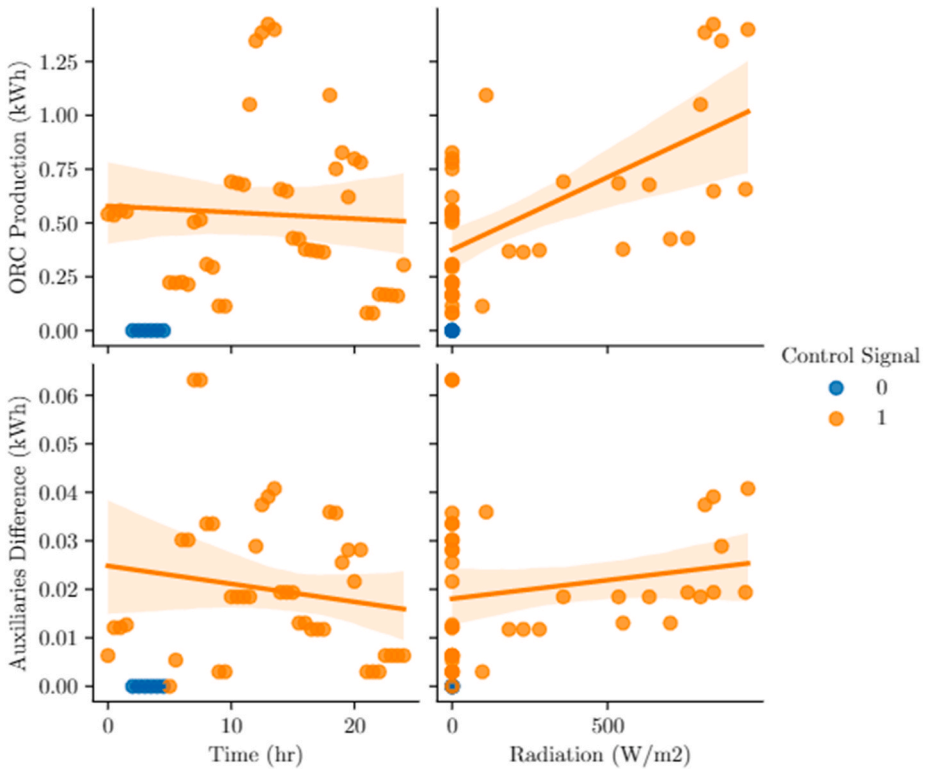

Fig. 13. ORC operation and difference of auxiliaries on 31st August in Seville.

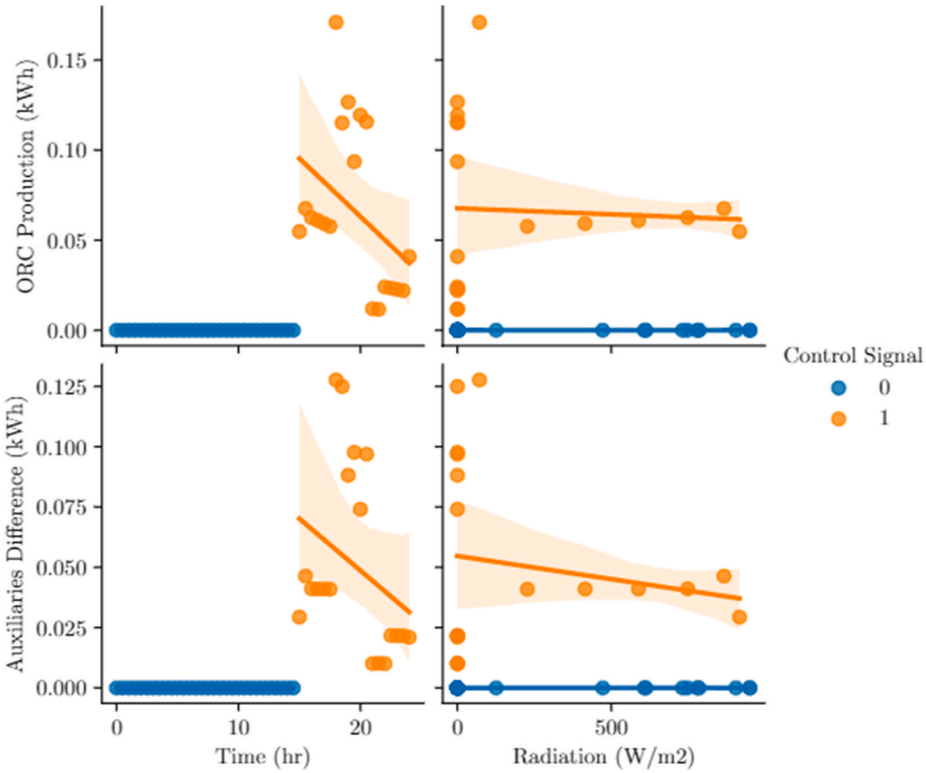

Fig. 14. ORC operation and difference of auxiliaries on 13th January in Seville.

decreases. Maximum peak production occurs at 13:00 for irradiation of 840 W/m^2, having a moderate demand.

However, this trend is much more pronounced in the case of a winter day (Fig. 14). Tank loading occurs throughout the day and the available resource is smaller. Thus, the ORC only produces in the last hours of the day and incurs significant differences in the auxiliaries. During these hours, the storage tank is discharged, resulting in lower demand, as estimated in Fig. 9.

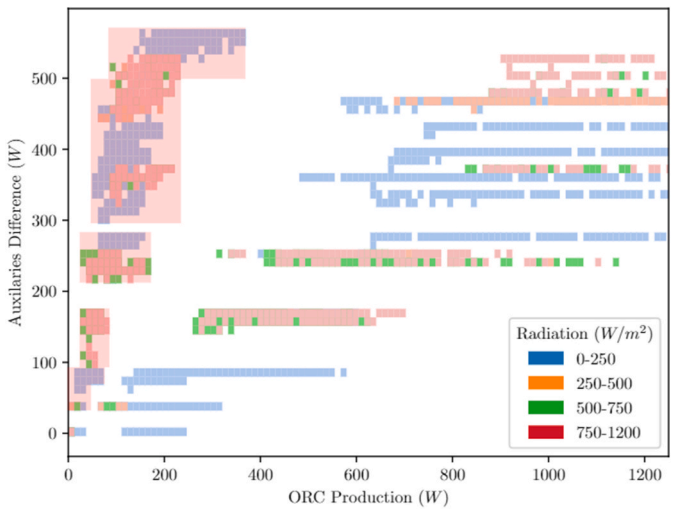

Fig. 15. Difference in auxiliary power due to ORC production by incident radiation ranges.

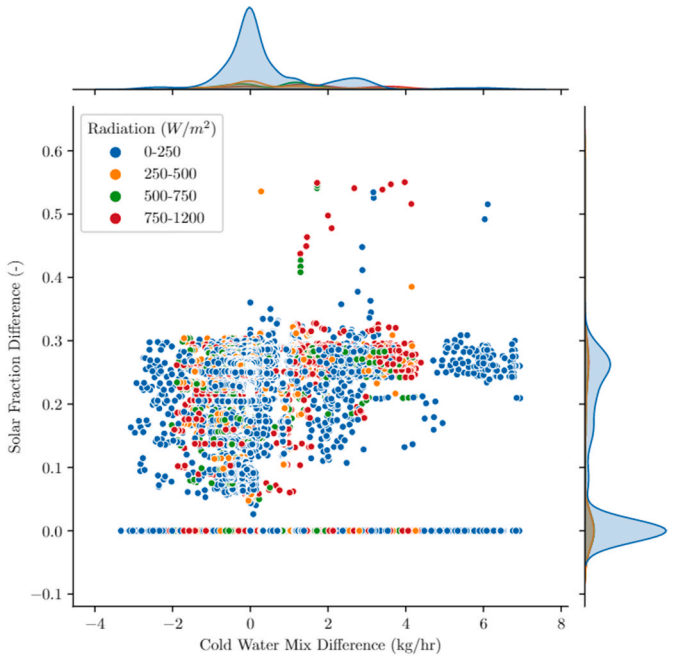

Fig. 16. Difference of solar fractions and cold-water mixing difference for different incident irradiation ranges.

Simulating in TRNSYS, the differences in the auxiliaries compared to the base case and the net ORC production are shown in Fig. 15. There are times when the difference in the auxiliaries compared to the base case is greater than the ORC output (red highlighted zone in Fig. 15). This is mainly because the circuit is associated with the DHW demand in the house, thus passing less water mass flow through the evaporator and cooling it more sharply. In these cases, the resource is insufficient, so the ORC penalises the installation. This usually occurs at times of the day when demand is low or when irradiation is low. Despite this no-feasibility zone, the ORC output is higher than the auxiliary difference for higher demands, resulting in a positive balance.

The thermal difference associated with the auxiliary difference will be quantified through the solar fraction. This parameter is an indicator of the contribution of solar collectors to water heating, including the auxiliary system. Fig. 16 shows the variation of the solar fraction as a function of the radiation range and the difference in the mixing

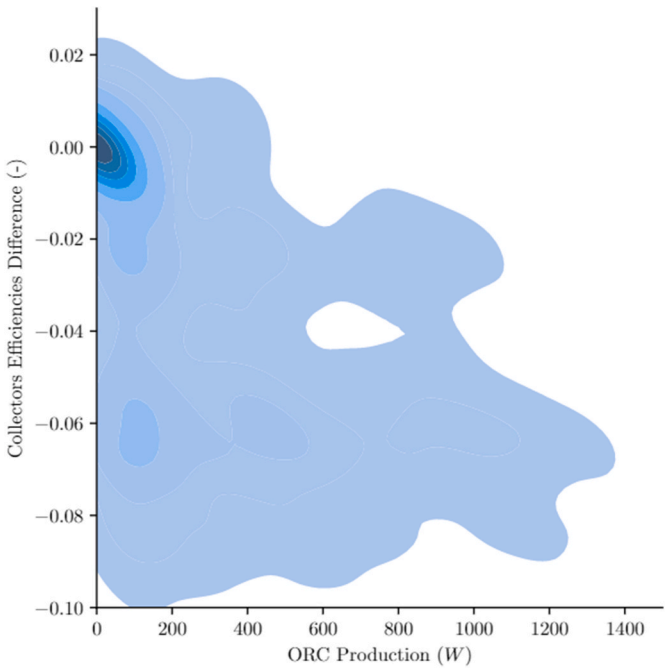

Fig. 17. Differences in solar collectors' efficiencies in terms of ORC expander production.

difference of cold water.

Fig. 16 shows how ORC can reduce the solar fraction by up to 30% in the summer months when the demand is typically lower, and the solar resource is higher. This leads to less mixing with cold water as the water temperature is lowered as it passes through the Rankine cycle. As the solar resource is higher, the difference in mixing cold water is also greater. This behaviour is more significant for higher irradiance, i.e., when there is a higher probability of excess thermal energy. The difference in the solar fractions for lower irradiance is practically nil, except at certain moments of low demand, when the storage temperature is higher than the set point and the ORC works at partial load due to the low water flow through its evaporator, penalising the global performance of the proposed installation. Therefore, there is a known synergy between the mass flow of cold water mixing and the collection efficiency. Performance is also penalised as more cold water is mixed in because less flow flows through the tank and the collectors.

As the cycle operates continuously for a more significant number of hours, the water flow throught the tank is greater, as the ORC decreases the temperature until the demand is met.

The usual adaptation behaviour shows positive results for the collector efficiency, up to 10% higher than in the base case, at times when the difference in the mixing water flow rate is greater than in the base case. Fig. 17 shows the difference in collection yields with respect to total ORC production, excluding pump consumption.

In performing the optimisation analysis, several operating points of the ORC have been proposed based on the temperature of the storage tank outlet. This fact determines the overall cost and efficiency of the cycle by determining the maximum temperature difference between the hot and cold sources. In this way, the cycle produces more hours per year but penalises the installation more sharply than when taking higher values for a lower set point. This also occurs with the total investment costs of the cycle, having implemented the thermo-economic analysis within the simulations.

4.1. Storage tank volume influence

Reducing the storage volume reduces losses and increases the outlet water temperature. This causes the solar fraction to decrease

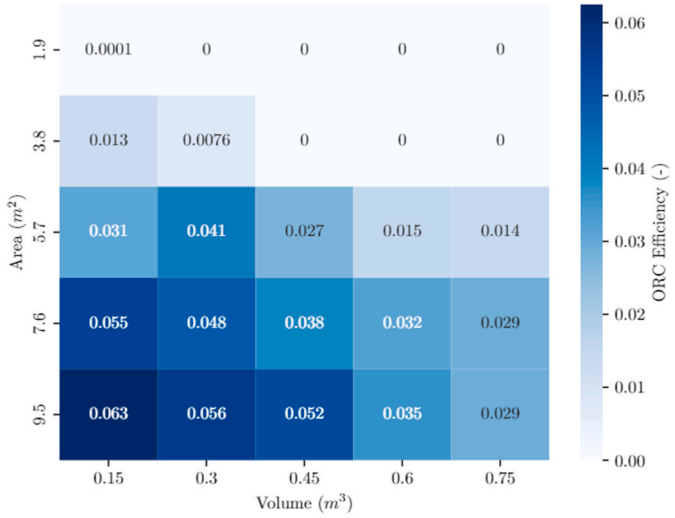

Fig. 18. ORC net efficiency as a function of collector area in square metres and storage volume in cubic metres.

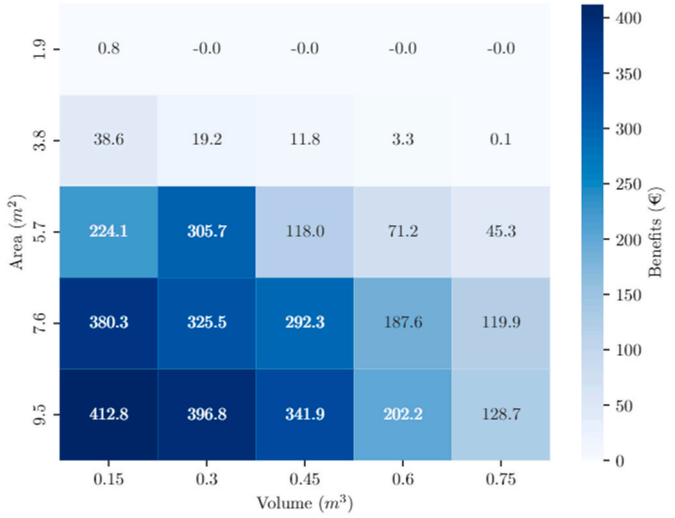

Fig. 19. SDHW-ORC Adaptation benefits as a function of collector area in square metres and storage volume in cubic metres.

considerably, penalising renewable generation by having less thermal storage, although the generation of electricity in the ORC is higher (and its efficiency) due to a higher water temperature at the outlet of the tank, as shown in Fig. 18.

From an economic point of view, it is the most convenient, but it is particularly sensitive to the cost of electricity and the variation in demand, so the decision would not be correct. Therefore, decisions are made in the second part of the profit heat map (Fig. 19), indicating positive economic parameters for volume-to-area ratios of 50–75 l/m^2.

The demand is calculated from the storage volume, which is 1.5 times the demand. It ensures that the circuit has a flow rate appropriate to the storage volume. However, this benefits the ORC, which operates with the same refrigerant mass flow rate as in the previous cases, but more water reaches the evaporator, ensuring more efficient production and, above all, greater continuity over time.

4.2. Economic analysis

Assembly costs are estimated to be 30–35% of the total cost of the plant. The parameters of economic analysis are given by the internal rate of change:

$$IRR = r \; when \sum_{i=1}^{25} \frac{CF_i}{(1+r)^i} = 0 \tag{20}$$

and the net present value:

$$\mathrm{NPV} = \sum_{i=1}^{25} \frac{\mathrm{CF_i}}{(1+\mathrm{r})^{\mathrm{i}}} \tag{21}$$

Thus, the outlet water temperature that produces the best internal rate of return and economic parameters is 80 °C, where the auxiliary difference is not too high with respect to the net production of ORC (Table 5). This analysis is carried out considering a discount rate of 7% and inflation of 2%. Maintenance costs are set at 2% per year of profit and replacement of the expander is considered every seven years.

It should be noted that the ORC produces at the point of greatest economic profitability for approximately 1496 h per year, indicating that for the installation studied, with a certain overdimension based on a high solar contribution mainly in the winter months, there is an excess of thermal energy from the collectors for 15% of the year. This excess is not only due to the summer months but is distributed between spring and summer in the case of Seville in Spain and the rest of the cities with a Mediterranean climate.

5. Conclusions

This paper has developed an analysis of the integration of an organic Rankine cycle within residential solar thermal installations. It has developed the stationary and dynamic models of the system based on using TRNSYS, yielding the following conclusions about retrofitting:

- The size of the ORC evaporator penalises the initial installation only when the demand is below 60% of the highest demand of the day, which usually occurs under conditions of low incident irradiation.
- Retrofitting benefits the solar installation by mixing less cold water (for single-family dwelling up to 8 kg/h compared to the base case) and bringing more water to the storage tank and the solar collectors. This improves the performance of the collectors by an average of 7.25% per year.
- Regarding the solar fractions, a decrease is shown, especially in the months of higher irradiation, which implies a recovery of residual heat without penalising the demand. Therefore, domestic hot water will be obtained at 40–45 °C, obtaining about 1 kWe net at the output of an organic Rankine cycle with R245fa as the working fluid.
- The economic parameters are positive for a Mediterranean climate with a high solar resource such as Seville. Both the net present value and the internal rate of return are close to the discount rate value, which implies that the investment is very close to being indifferent. The viability of the retrofit is strongly dependent on electricity prices due to the variability of solar radiation and the demand for DHW,

Table 5
Results according to Set Point of water temperature at the outlet of the storage.

Set Point (°C)	ORC Production (kWh)	Net Auxiliaries Difference (kWh)	Net Cycle Efficiency (%)	NPV (€)	IRR (%)	SC (€/kW)	Solar Fraction (%)
75	1475.82	120.47	4.10	315.77	8.25	2739.62	65.73
80	1495.78	96.63	5.40	392.69	8.61	2638.79	70.34
85	1189.37	72.55	5.53	454.8	8.57	2539.16	72.60

which affect the outlet temperature of the collector water and the input water to the ORC evaporator, respectively.
- As the storage is greater, inertia is also greater for this low-demand installation, and so are the losses, and decrease in the temperature at the outlet penalising the organic Rankine cycle.
- According to current Spanish regulations and global trends, the ratio between storage volume in litres and solar field area in square metres that provides the greatest benefit is between 50 and 75 l/m^2.
- The challenge for this integration is developing reliable moderate-cost systems to ensure cost-effective thermal/electrical integration.

Credit author statement

D.A Rodríguez-Pastor: Investigation, Conceptualisation, Methodology, Writing e original draft. R. Chacartegui: Methodology, Conceptualisation, Supervision, Writing. J.A Becerra: Funding acquisition, Supervision.

Abbreviations

DHW	Domestic Hot Water
CF	Cash Flow
CHP	Combined Heat and Power
IRR	Internal Rate of Return
NPV	Net Present Value
ORC:	Organic Rankine Cycle
SDHW	Solar Domestic Hot Water
SC:	Specific Costs

Superscripts and subscripts

cd:	condensation
coll	solar collector
div:	diverter
ev:	evaporation
ex:	exhaust
exp	expander
fr:	friction
in:	inlet
is:	isentropic
l:	saturated liquid
m:	mean
nom	nominal
out	outlet
p	water pump
pump:	ORC pump
ref:	refrigerant (working fluid)
su	supply
tp	two-phase
v:	saturated vapour
vol	volumetric
w:	water

Notation

η:	cycle efficiency [-]
$\dot{Q}$:	thermal power [W]
$\dot{W}$:	mechanical power [W]
Nu:	Nusselt number $Nu = \frac{\alpha L}{k}$ [-]
β':	Chevron angle ratio $\frac{\beta}{\beta_{max}}$ [-]
Pr:	Prandlt number $Pr = \frac{\mu c_p}{k}$ [-]
Re:	Reynolds number $Re = \frac{\rho u L}{\mu}$ [-]
Bd:	Bond number $Bd = \frac{g L^2 (\rho_l - \rho_v)}{\sigma}$ [-]
Bo:	Boiling number $Bo = \frac{\dot{q}}{\Delta G i_{fg}}$ [-]

Declaration of competing interest

The authors declare that they have no known competing financial interests or personal relationships that could have appeared to influence the work reported in this paper.

Data availability

Data will be made available on request.

Acknowledgements

This work was partially funded by the project "Rediseño y adaptación de caldera diésel HT para trabajo a baja potencia", reference FIUS20/0123, by the Research Foundation of the University of Seville.

ρ: density [kg/m^3]
f: friction factor or fraction [-]
G: specific mass flow $G = \rho u$ [kg/m^2-s]
We Weber number $We = \frac{\rho u^2 L}{\sigma}$ [-]
g: gravity number 9.81 [m/s^2]
p: pressure [Pa]
α: heat transfer coefficient [W/m^2-K]
μ: viscosity [Pa·s]
σ: interfacial surface tension [N/m]
u: velocity [m/s]
L: characteristic length [m]
c_p: specific heat [J/kg-K]
$\dot{m}$: mass flow rate [kg/s]
T: temperature [°C]
C: heat capacitance $C = \dot{m}c_p$ [W/K]
N: rotational speed [rpm]
ε: efficiency [-]
I: solar irradiation [W/m^2]
V: volume [m^3]
U: global heat transfer coefficient [W/m^2-K]
v: specific volume [m^3/kg]
CF: cash flow [€]

References

[1] Fawcett T, Topouzi M. Energy policy for buildings fit for the future. In: Research handbook on energy and society. Edward Elgar Publishing; 2021.
[2] Programme UNE. Global status report for buildings and construction: towards a zero-emission, efficient and resilient buildings and construction sector. 2021 [Online]. Available: www.globalabc.org.
[3] Zachmann G, et al. Decarbonisation of the energy system. 2022.
[4] Fajardy M, Reiner DM. Electrification of residential and commercial heating. In: Handbook on electricity markets. Edward Elgar Publishing; 2021.
[5] Louvet Y, et al. Economic comparison of reference solar thermal systems for households in five European countries. Sol Energy 2019;193:85–94.
[6] of Development M. "Código Técnico de la Edificación. G. of S. Basic document HE - Energy savings; 2019.
[7] ASIT. Report on the Spanish solar thermal market," madrid. 2021 [Online]. Available: https://www.asit-solar.com/.
[8] Weiss W, Spörk-Dür M. Solar heat worldwide 2020 - global market development and trends in 2019. Sci. Technol. Built Environ. 2019;24(8):819.
[9] Qyyum MA, et al. Assessment of working fluids, thermal resources and cooling utilities for Organic Rankine Cycles: state-of-the-art comparison, challenges, commercial status, and future prospects. Energy Convers Manag 2022;252:115055. https://doi.org/10.1016/j.enconman.2021.115055.
[10] Rahbar K, Mahmoud S, Al-Dadah RK, Moazami N, Mirhadizadeh SA. Review of organic Rankine cycle for small-scale applications. Energy Convers Manag 2017; 134:135–55. https://doi.org/10.1016/j.enconman.2016.12.023.
[11] Ancona MA, et al. Solar driven micro-ORC system assessment for residential application. Renew Energy 2022;195:167–81. https://doi.org/10.1016/j.renene.2022.06.007.
[12] Pereira JS, Ribeiro JB, Mendes R, Vaz GC, André JC. ORC based micro-cogeneration systems for residential application – a state of the art review and current challenges. Renew Sustain Energy Rev 2018;92:728–43. https://doi.org/10.1016/j.rser.2018.04.039.
[13] Pei G, Li J, Ji J. Analysis of low temperature solar thermal electric generation using regenerative Organic Rankine Cycle. Appl Therm Eng 2010;30(8–9):998–1004.
[14] Antonelli M, Baccioli A, Francesconi M, Lensi R, Martorano L. Analysis of a low concentration solar plant with compound parabolic collectors and a rotary expander for electricity generation. Energy Proc 2014;45:170–9.
[15] Arteconi A, del Zotto L, Tascioni R, Cioccolanti L. Modelling system integration of a micro solar Organic Rankine Cycle plant into a residential building. Appl Energy 2019;251:113408. https://doi.org/10.1016/J.APENERGY.2019.113408.
[16] Cioccolanti L, Villarini M, Tascioni R, Bocci E. Performance assessment of a solar trigeneration system for residential applications by means of a modelling study. Energy Proc Oct. 2017;126:445–52. https://doi.org/10.1016/j.egypro.2017.08.211.
[17] Lombardo W, Sapienza A, Ottaviano S, Branchini L, de Pascale A, Vasta S. A CCHP system based on ORC cogenerator and adsorption chiller experimental prototypes: energy and economic analysis for NZEB applications. Appl Therm Eng 2021;183 (Oct). https://doi.org/10.1016/j.applthermaleng.2020.116119.
[18] S. Martinez, G. Michaux, J.L. Bouvier, and P. Salagnac, "Numerical investigation of the energy performance of a solar micro-CHP unit," Energy Convers Manag, vol. 243, p. 114425, Oct. 2021, doi: 10.1016/J.ENCONMAN.2021.114425.
[19] Villarini M, Tascioni R, Arteconi A, Cioccolanti L. Influence of the incident radiation on the energy performance of two small-scale solar Organic Rankine Cycle trigenerative systems: a simulation analysis. Appl Energy 2019;242: 1176–1188, Oct. https://doi.org/10.1016/J.APENERGY.2019.03.066.
[20] J. Lizana, C. Bordin, and T. Rajabloo, "Integration of solar latent heat storage towards optimal small-scale combined heat and power generation by Organic Rankine Cycle," J Energy Storage, vol. 29, p. 101367 Oct. 2020, doi: 10.1016/J.EST.2020.101367.
[21] Wang RQ, Jiang L, Wang YD, Roskilly AP. Energy saving technologies and mass-thermal network optimization for decarbonized iron and steel industry: a review. J Clean Prod 2020;274:122997. https://doi.org/10.1016/j.jclepro.2020.122997.
[22] Z. Özcan and Ö. Ekici, "A novel working fluid selection and waste heat recovery by an exergoeconomic approach for a geothermally sourced ORC system," Geothermics, vol. 95, p. 102151, Oct. 2021, doi: 10.1016/J.GEOTHERMICS.2021.102151.
[23] Rodriguez DA, Chacartegui R, Becerra JA. Proyecto Fin de Carrera Ingeniería de la Energía Adaptación de sistemas residenciales de energía solar para ACS a la generación distribuida híbrida mediante ORC. 2021.
[24] Chacartegui R, Becerra JA, Blanco MJ, Muñoz-Escalona JM. A humid air turbine–organic rankine cycle combined cycle for distributed microgeneration. Energy Convers Manag Oct. 2015;104:115–26. https://doi.org/10.1016/J.ENCONMAN.2015.06.064.
[25] ATECYR, *Technical Guide*. Central domestic hot water. 2010.
[26] METEONORM. Handbook part II (7) : theory global meteorological database version 7 software and data for engineers , planers and education," handb. Part II theory. no. January; 2019.
[27] Klein SA. Operating Manual.Engineering equation solver (EES). 2007 [Online]. Available: http://www.fchart.com/ees/.
[28] Bull J, Buick JM, Radulovic J. Heat exchanger sizing for organic rankine cycle. Energies 2020;13:14. https://doi.org/10.3390/en13143615.
[29] Amalfi RL, Vakili-Farahani F, Thome JR. Flow boiling and frictional pressure gradients in plate heat exchangers. Part 2: comparison of literature methods to database and new prediction methods. Int J Refrig 2016;61:185–203. https://doi.org/10.1016/j.ijrefrig.2015.07.009.
[30] García-Cascales JR, Vera-García F, Corberán-Salvador JM, Gonzálvez-Maciá J. Assessment of boiling and condensation heat transfer correlations in the modelling of plate heat exchangers. Int J Refrig 2007;30(6):1029–41. https://doi.org/10.1016/j.ijrefrig.2007.01.004.
[31] Lemort V, Quoilin S, Cuevas C, Lebrun J. Testing and modeling a scroll expander integrated into an Organic Rankine Cycle. Appl Therm Eng 2009;29(14–15): 3094–102. https://doi.org/10.1016/j.applthermaleng.2009.04.013.
[32] Garcia-Saez I, Méndez J, Ortiz C, Loncar D, Becerra JA, Chacartegui R. Energy and economic assessment of solar Organic Rankine Cycle for combined heat and power generation in residential applications. Renew Energy 2019;140:461–76. https://doi.org/10.1016/j.renene.2019.03.033.
[33] Quoilin S. 21_Sustainable energy conversion through the use of organic rankine cycles for waste heat recovery and solar applications. Belgium: Sylvain Quoilin, University of Liège; 2008. October, 2011.
[34] Dickes R, Dumont O, Legros A, Quoilin S, Lemort V. Analysis and comparison of different modeling approaches for the simulation of a micro-scale organic Rankine cycle power plant. Proc. ASME -ORC 2015;2015.
[35] Longo GA, Righetti G, Zilio C. A new computational procedure for refrigerant condensation inside herringbone-type Brazed Plate Heat Exchangers. Int J Heat Mass Tran 2015;82:530–6. https://doi.org/10.1016/j.ijheatmasstransfer.2014.11.032.

[36] Yam YY, Lin TF, Yang BC. Evaporation heat transfer and pressure drop of refrigerant R134a in a plate heat exchanger. Proc. ASME Turbo Expo 1997. https://doi.org/10.1115/97-AA-048.
[37] Declaye S, Quoilin S, Guillaume L, Lemort V. Experimental study on an open-drive scroll expander integrated into an ORC (Organic Rankine Cycle) system with R245fa as working fluid. Energy 2013;55:173–83. https://doi.org/10.1016/j.energy.2013.04.003.
[38] Bell IH, Wronski J, Quoilin S, Lemort V. Pure and pseudo-pure fluid thermophysical property evaluation and the open-source thermophysical property library coolprop. Ind Eng Chem Res 2014;53(6):2498–508. https://doi.org/10.1021/ie4033999.
[39] A Klein S. TRNSYS 18: a transient system simulation program. Madison, USA: Solar Energy Laboratory, University of Wisconsin; 2017 [Online]. Available: http://sel.me.wisc.edu/trnsys.
[40] TESS COMPONENT LIBRARIES volume 7. The Hydronic Component Library," TRNSYS17 Doc.; 2014. p. 1–79.
[41] OMIE. Iberian electricity market evolution. In: Annual report; 2020.